



Contents lists available at ScienceDirect

International Journal of Applied Earth Observation and Geoinformation

journal homepage: www.elsevier.com/locate/jag



GEMMA: An Earth crustal model based on GOCE satellite data

M. Reguzzoni^a, D. Sampietro^{b,*}

^a DICA – Politecnico di Milano, Piazza Leonardo da Vinci 32, 20133 Milano, Italy

^b GReD s.r.l., Via Valleggio 11, 22100 Como, Italy

ARTICLE INFO

Article history:

Available online xxx

Keywords:

Earth crustal model
Global Moho model
GOCE satellite
Inverse gravimetric problem

ABSTRACT

The boundary between Earth's crust and mantle is commonly modelled as a discontinuity surface, the so-called Moho. Although in some regions of the world this model may be too approximate or even unrealistic, globally speaking it can provide a key to read several long wavelength geophysical signals. Recent research activities have shown the possibility to estimate the Moho discontinuity worldwide from global gravity field model, however usually the solution of this inverse problem requires strong unrealistic hypotheses.

In this work a new procedure to relax some of these unrealistic hypotheses is devised and described in details. Basically it allows to estimate the mean Moho depth even once the normal gravitational field is removed if at least one seismic observation is available, to take into account the dependency of the crust density on the radial direction (usually neglected in Moho depth determination from gravity), to correct the a-priori density model of the crystalline crust for scale factors again using seismic information and finally to consider a Moho with a non-constant depth as reference surface in the inversion, thus reducing the linearization error.

The new procedure is here applied to GOCE data to estimate a new crustal model. For this purpose additional external information has been used, such as topography, bathymetry and ice sheet models from ETOPO1, a recent $1^\circ \times 1^\circ$ sediment global model and some prior hypotheses on crustal density. In particular the main geological provinces, each of them characterized by its own relation between density and depth, have been considered. A model describing lateral density variations of the upper mantle is also taken into account.

The new crustal model is computed at a spatial resolution of $0.5^\circ \times 0.5^\circ$, its gravitational effect differs from GOCE observations of 49 mE and its Moho depth error standard deviation is globally of 3.4 km. Therefore the result seems to be an improvement in terms of resolution, consistency with the gravity field and accuracy not only with respect to previously released GEMMA models, but also with respect to the current state-of-the-art global knowledge of the Earth crust.

© 2014 Elsevier B.V. All rights reserved.

1. Introduction

For the first time with the ESA Earth explorer GOCE mission (Drinkwater et al., 2003), thanks to its innovative on-board gradiometer and its extremely low orbit, a high resolution image of the Earth steady state gravitational field has been globally observed with high accuracy (Pail et al., 2011). Among other applications, like improving climate models by providing new information on ocean circulation and sea level (Knudsen et al., 2011) or underpinning a global geodetic height datum (Rummel, 2012; Gatti et al., 2013), also the study of the boundary between the Earth crust

and mantle, classically modelled as a discontinuity surface called Mohorovičić discontinuity or Moho (Fowler, 1990), can take advantage of the newly available observations. In order to have a glimpse on how accurate this dataset is, one can think for example to the fact that the Moho depth can be theoretically recovered from GOCE gravity gradients (considering the observation noise only and neglecting the error due to the use of non-exact geophysical models for the data reduction) at a level of 0.1 km uncertainty with a resolution better than $1^\circ \times 1^\circ$ almost worldwide (Braatenberg et al., 2011; Reguzzoni and Sampietro, 2012). This improvement in accuracy and resolution in the description of the gravity field should be followed by a parallel enhancement in the modeling and in the assumptions required for the recovery of the Moho depth from gravity observations. Moho models derived from gravity, such those presented in Sünkel (1985), Moritz (1990), Sjöberg (2009)

* Corresponding author. Tel.: +39 0313327522.

E-mail address: daniele.sampietro@g-red.eu (D. Sampietro).

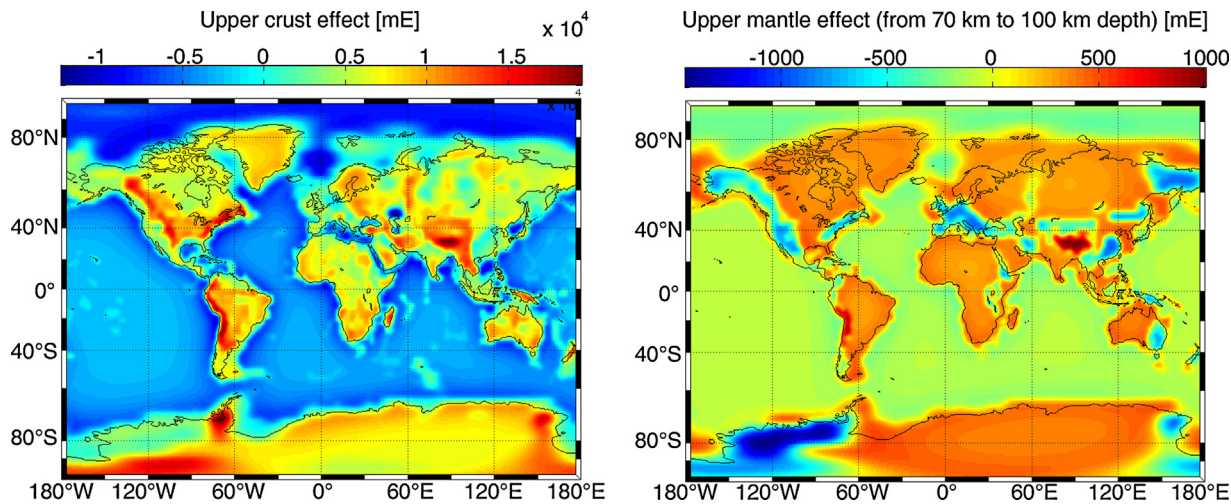


Fig. 1. Gravitational effect in terms of second radial derivatives of the gravitational potential at GOCE mean altitude due to the CRUST2.0 upper crust (left) and to the lateral density variation inside the mantle (right). Mean values have been removed.

and Reguzzoni et al. (2013), are usually based on very simplifying hypotheses, e.g. crustal densities not dependent on depth or even constant. In addition, the problem of introducing seismic information into Moho models computed from gravimetric observations, see for instance Sjöberg and Bagherbandi (2011) and more recently Reguzzoni et al. (2013) at a global scale or Sampietro et al. (2014) at a regional one, is a challenging task since the hypotheses underlying the seismic and gravimetric methods are in general different and complementary. For example the combination proposed in Sjöberg and Bagherbandi (2011) and Reguzzoni et al. (2013), where a global Moho model derived from gravity observations is a-posteriori combined with a seismic derived one, will lead to a solution in which the consistency with the gravitational field and even with the crustal model used to reduce gravity data is not guaranteed. Moreover the combination between gravity and seismic is made more complicated by the fact that a complete description of the error of the different information sources is generally not available. In this work a new global crustal model, developed in the framework of the ESA-STSE GEMMA project (GOCE Exploitation for Moho Modeling and Applications) and called GEMMA1.0, is presented. It is based on GOCE data, on an accurate description of the crustal structure and on some prior seismic information. In Section 2, after recalling for the sake of completeness the main concepts and definitions, the proposed inversion algorithm is presented: in details in Section 2.1 a first improvement with respect to what presented in Reguzzoni et al. (2013) regarding the mean Moho depth estimation is described, while in Section 2.2 the inversion algorithm is further enhanced in order to allow the use of a crustal density model with radial variations in the data reduction, thus overcoming another limitation of the inversion presented in Reguzzoni et al. (2013). This is a crucial issue since, as it is well known in literature, the variation of crustal density with respect to depth can reach values larger than 300 kg/m³. After that the possibility to combine the gravitational observations with seismic derived data (not only for the mean Moho estimation) is described in Section 2.3: differently from the combination presented in Reguzzoni et al. (2013), the solution discussed here is not a weighted average between a GOCE-only Moho and the CRUST2.0 one (Bassin et al., 2000), but it is a solution practically independent from CRUST2.0 that is used just to estimate few parameters, such as scale factors of the crustal density model. Note that the proposed solution guarantees the consistency of the resulting crustal model with the gravitational field. In Section 2.4 the possibility to iterate the inversion algorithm is depicted. Again this represents a major improvement with respect to Reguzzoni

et al. (2013) since it gives the possibility to compute a Moho undulation not only with respect to a constant Moho depth, but also with respect to a surface closer to the expected solution. Finally in Section 3 the above inversion algorithm is applied to GOCE data, while in Section 4 comparisons with other existing global models are shown and some conclusions are drawn too.

2. The inversion algorithm

The proposed inversion algorithm is essentially based on five different steps. In the first one a global grid of a functional of the Earth gravitational potential, to fix the idea we can think to a grid of second radial derivatives of the gravitational potential from GOCE at mean satellite altitude, is reduced to the gravitational effect of the masses between the actual and a constant reference Moho. In the second step a spherical harmonic analysis operator is applied to the reduced grid in order to estimate a set of spherical harmonic coefficients δT_{nm} ; in particular they are computed as in Colombo (1981) or Reguzzoni (Italy). In the third step an inversion operator is applied to these coefficients. This is based on a linearized expression (Strang van Hees, 2000; Reguzzoni et al., 2013) that relates δT_{nm} to the coefficients $\delta \omega_{nm}$ of a functional $\delta \omega(\varphi, \lambda)$ defined as the product between the Moho undulation $\delta D(\varphi, \lambda)$ and its density contrast $\Delta \rho(\varphi, \lambda)$:

$$\delta \omega(\varphi, \lambda) = \delta D(\varphi, \lambda) \Delta \rho(\varphi, \lambda) \quad (1)$$

where φ is the latitude and λ is the longitude. The Moho undulation is referred to a constant reference Moho of radius $R_E - \bar{D}$ (where R_E is the mean Earth radius and \bar{D} is the depth of the reference Moho, i.e. the linearization point used). Mathematically speaking it turns out that:

$$\delta \omega_{nm} = \rho_E (R_E - \bar{D}) \beta_n \delta T_{nm} \quad (2)$$

$$\beta_n = -\frac{(2n+1)}{(1 - (\bar{D}/R_E))^{n+3}} \quad (3)$$

ρ_E being the mean Earth mass density. Note that the estimated coefficients of Eq. (2) are (a posteriori) regularized in order to bound the signal power of the resulting Moho at the highest degrees (above degree 160). For details on the regularization the reader can refer to Reguzzoni et al. (2013). A spherical harmonic synthesis is then applied (fourth step) to get a geographical grid of $\delta \omega(\varphi,$

λ), from which the Moho undulation can be estimated by simply dividing by the assumed density contrast (fifth step):

$$\delta D(\varphi, \lambda) = \frac{\delta\omega(\varphi, \lambda)}{\Delta\rho(\varphi, \lambda)}. \quad (4)$$

The Moho depth $D(\varphi, \lambda)$ can be finally estimated as:

$$D(\varphi, \lambda) = \delta D(\varphi, \lambda) + \bar{D}. \quad (5)$$

The whole procedure (actually from the second to the fifth step) can be seen as an inversion operator $\mathcal{I}_0(\cdot)$, that is linearized around a reference Moho depth \bar{D} and that, given a properly reduced signal $\delta T_{rr}^{\bar{D}}(\varphi, \lambda)$ with respect to the same reference Moho and a density contrast $\Delta\rho(\varphi, \lambda)$, returns the corresponding Moho depth:

$$D(\varphi, \lambda) = \mathcal{I}_0 \left(\delta T_{rr}^{\bar{D}}(\varphi, \lambda), \Delta\rho(\varphi, \lambda) \right). \quad (6)$$

As stated above, before inverting gravity data it is necessary to remove the gravitational signal of all the masses from the observations, apart from those between the reference Moho and the actual one. In this framework the original observations can be first reduced to anomalous quantities by subtracting the contribution of the normal potential. This can be interpreted as the subtraction of the contribution of the global Earth mass assuming that it is homogeneously distributed over layers with ellipsoidal boundaries. The residual signal of this initial step can be therefore considered as the effect of density anomalies inside each layer and the effect of non-ellipsoidal boundaries between contiguous layers. It should be noted that once the data are reduced to the anomalous field it is no more possible to estimate the mean depth of the Moho, as discussed in Reguzzoni et al. (2013) and recalled in Section 2.1. After that, the gravitational contribution of any mass anomaly from the top of the topography (including ice sheets) to the crystalline basement are assumed to be known without any uncertainties and are removed from the data:

$$T_{rr}^{\text{RES}} = T_{rr}^{\text{OBS}} - T_{rr}^{\text{ICE}} - T_{rr}^{\text{OCE}} - T_{rr}^{\text{SED}} \quad (7)$$

where T_{rr}^{OBS} is the observed grid of second radial derivatives of the anomalous potential, T_{rr}^{ICE} is the effect of ice sheets assuming to know their density and geometrical shape, T_{rr}^{OCE} is the effect of oceanic masses assuming a known water density and bathymetry and T_{rr}^{SED} is the effect of sediments. The dependence of these gravity data on φ and λ is omitted for the sake of simplicity. The gravitational attraction of each layer ℓ is computed by applying a forward operator $\mathcal{F}(\cdot)$, e.g. based on point masses numerical integration, to each density model $\rho^\ell(\varphi, \lambda, r)$ knowing the boundary of each layer, i.e. the depth of its bottom $D_B^\ell(\varphi, \lambda)$ and top $D_T^\ell(\varphi, \lambda)$:

$$T_{rr}^\ell = \mathcal{F}(\rho^\ell(\varphi, \lambda, r), D_B^\ell, D_T^\ell), \quad (8)$$

where r is the radial coordinate. Like for the gravity data, the dependence of the layer boundaries on φ and λ in the forward operator is omitted for the sake of simplicity.

In order to reduce the T_{rr}^{RES} to the effect of the Moho undulation only, the signal due to the density anomalies in the crystalline crust T_{rr}^{CRUST} and in the upper mantle T_{rr}^{MANTLE} should be also removed:

$$\delta T_{rr}^{\bar{D}} = T_{rr}^{\text{RES}} - T_{rr}^{\text{MANTLE}} - T_{rr}^{\text{CRUST}}. \quad (9)$$

where both T_{rr}^{CRUST} and T_{rr}^{MANTLE} should be computed using a reference Moho at a constant depth \bar{D} .

It should be stressed that the choice of $\rho^{\text{CRUST}}(\varphi, \lambda, r)$ and $\rho^{\text{MANTLE}}(\varphi, \lambda, r)$ is a critical factor in the inversion procedure: they are required in order to reduce gravity observations (like all the other density models), but they also implicitly define the density contrast at the Moho to be used in Eq. (4). As for $\rho^{\text{CRUST}}(\varphi, \lambda, r)$ we suppose here to divide the whole Earth in M geologically homogeneous patches, each of them classified as one of the main crustal

types (i.e. shield, platform, etc.). A specific crustal density is thus assumed for each type of province. The computation of the gravitational effect of the upper mantle requires to define the mantle density and its lower boundary. The latter should be a reference surface at a constant depth, lower than the minimum Moho depth. Although less known, the impact of the upper mantle density variation is significantly smaller than the one of the crystalline crust (see e.g. Fig. 1 where the effect of the upper crust is compared with the one of the lateral density variation in the mantle at a depth between 70 km and 100 km): this is due in part to the fact that the mantle is a deeper layer and in part to its greater homogeneity. For these reasons, from now on, we will assume that the upper mantle density is $\rho^{\text{MANTLE}}(\varphi, \lambda)$, disregarding any radial variation down to its lower boundary.

Once data have been reduced, \mathcal{I}_0 can be applied and the Moho depth is recovered. For details on the hypotheses required by the inversion algorithm and the corresponding errors the reader can refer to Reguzzoni et al. (2013), we just remind here that there are four main drawbacks in this procedure:

1. The fact that the mean Moho depth cannot be estimated without making a hypothesis on the mass density distribution of all the Earth, from the core to the topography;
2. The fact that the actual crustal density depends on the radial direction but the density contrast $\Delta\rho$ used in the operator \mathcal{I}_0 must be a function of latitude and longitude only;
3. The fact that the density model of each layer, but in particular the one of the crystalline crust, is considered perfectly known;
4. The fact that the operator \mathcal{I}_0 is linearized with respect to a reference Moho at a constant depth \bar{D} , which could be very far from the actual one.

In the following subsections \mathcal{I}_0 will be improved in order to overcome these limitations.

2.1. Mean Moho depth estimation

The estimation of the mean Moho depth from gravity data is a difficult (and practically impossible) task. In fact, once the normal potential has been removed, in principle one can only estimate a zero mean undulation of the Moho with respect to an a priori constant Moho depth. In essence, this is due to the fact that given the total Earth mass and chosen the reference ellipsoid (e.g. WGS84), there exists one and only one normal potential (Heiskanen and Moritz, 1999) but infinite mass distributions inside the ellipsoid generating the same normal potential. For any possible crustal and upper mantle mass distribution of the normal potential one gets different density anomalies of T_{rr}^{ICE} , T_{rr}^{OCE} , T_{rr}^{SED} , T_{rr}^{CRUST} and T_{rr}^{MANTLE} , and therefore different $\delta T_{rr}^{\bar{D}}$ residuals from Eq. (9); however these residuals differ from one another for the mean value only. In other words, without making hypotheses on the mass distribution of the whole Earth, e.g. using PREM (Dziewonski and Anderson, 1981), the mean value of $\delta T_{rr}^{\bar{D}}$ is unknown and, consequently from Eqs. (2) and (4), the mean values of $\delta\omega(\varphi, \lambda)$ and $\delta D(\varphi, \lambda)$ are unknown too.

In order to solve this problem a constant parameter μ_ω is added to Eq. (5) obtaining:

$$D(\varphi, \lambda) = \frac{\delta\omega(\varphi, \lambda) + \mu_\omega}{\Delta\rho(\varphi, \lambda)} + \bar{D}. \quad (10)$$

The simplest solution to estimate μ_ω is to use external observations (e.g. from seismic data): if we suppose to know or observe the depth of the Moho at least in one point we can rearrange Eq. (10) in the following form:

$$\mu_\omega = [D_n^{\text{OBS}}(\varphi_n, \lambda_n) - \bar{D}] \Delta\rho(\varphi_n, \lambda_n) - \delta\omega(\varphi_n, \lambda_n) \quad (11)$$

where D_n^{OBS} is the observed Moho depth at the point of coordinates (φ_n, λ_n) . If the Moho is known from seismic in more than one point, the system of Eq. (11) can be solved by means of a least squares principle.

In this way a new inversion operator, depending on the μ_ω parameter too, is defined:

$$D(\varphi, \lambda) = \mathcal{I}_1 \left(\delta T_{rr}^{\bar{D}}(\varphi, \lambda), \Delta \rho(\varphi, \lambda), \mu_\omega \right). \quad (12)$$

2.2. Crustal density variation in the radial direction

The second approximation implied by \mathcal{I}_0 , i.e. the fact that $\Delta \rho$ is supposed to be a function of latitude and longitude only, is now considered. It is important to stress here that the crustal density variation with depth is a fundamental parameter in the Moho estimation: the density variation between upper and lower crust can reach, e.g. in orogenic crust, values larger than 300 kg/m^3 (Christensen and Mooney, 1995) thus considerably modifying the data reduction but, even more important, halving the density contrast between crust and mantle. In order to compute a solution with radial variations of crustal densities, Eq. (10) is simply modified in:

$$D(\varphi, \lambda) = \frac{\delta \omega(\varphi, \lambda) + \mu_\omega}{\rho^{\text{MANTLE}}(\varphi, \lambda) - \bar{\rho}^{\text{CRUST}}(\varphi, \lambda)} + \bar{D} \quad (13)$$

where $\bar{\rho}^{\text{CRUST}}(\varphi, \lambda)$ is computed as the mean density in the Moho undulation, i.e. the mean density between the constant reference Moho used as linearization point \bar{D} and the actual Moho $D(\varphi, \lambda)$:

$$\bar{\rho}^{\text{CRUST}}(\varphi, \lambda) = \frac{1}{D(\varphi, \lambda) - \bar{D}} \int_{\bar{D}}^{D(\varphi, \lambda)} \rho^{\text{CRUST}}(\varphi, \lambda, r) dr. \quad (14)$$

Practically the algorithm substitutes $\rho^{\text{CRUST}}(\varphi, \lambda, r)$ with $\bar{\rho}^{\text{CRUST}}(\varphi, \lambda)$ between \bar{D} and $D^+(\varphi, \lambda)$ in the data reduction, which means that:

$$T_{rr}^{\text{CRUST}} = \mathcal{F}(\rho^{\text{CRUST}}(\varphi, \lambda, r), \bar{D}, D_T^{\text{CRUST}}) + \mathcal{F}(\bar{\rho}^{\text{CRUST}}(\varphi, \lambda, r) - \rho^{\text{CRUST}}(\varphi, \lambda, r), \bar{D}, D^+). \quad (15)$$

where $D^+(\varphi, \lambda)$ is the depth of the Moho above the reference surface, i.e.

$$D^+(\varphi, \lambda) = \begin{cases} D(\varphi, \lambda) & \text{if } D(\varphi, \lambda) > \bar{D} \\ \bar{D} & \text{if } D(\varphi, \lambda) \leq \bar{D} \end{cases}. \quad (16)$$

In other words, since the inversion operator is anyhow linearized around a constant reference Moho and the preliminary data reduction has to be consistent with this reference Moho, the correction to T_{rr}^{CRUST} can be only computed for the upper part of the Moho. This pushes us to choose the reference Moho as low as possible and to disregard radial variations of the crustal densities below it (see Section 3).

It should be observed that both $\bar{\rho}^{\text{CRUST}}(\varphi, \lambda)$ and T_{rr}^{CRUST} are defined only once a Moho depth $D(\varphi, \lambda)$ is known. In order to compute a solution, an iterative algorithm is therefore setup, i.e.

$$D^{(t+1)}(\varphi, \lambda) = \mathcal{I}_2 \left(\delta T_{rr}^{\bar{D}}(\varphi, \lambda), \Delta \rho(\varphi, \lambda), D^{(t)}(\varphi, \lambda), \mu_\omega \right). \quad (17)$$

The algorithm is initialized by setting $D^{(t=0)} = \bar{D}$ and a prior mean crustal density $\bar{\rho}^{\text{CRUST}}(\varphi, \lambda)$. Knowing $D^{(t=0)}$ it is possible to compute T_{rr}^{CRUST} from Eq. (15), reduce and invert the gravitational observations to obtain $\delta \omega$, estimate μ_ω using the external information and finally compute $D^{(t=1)}(\varphi, \lambda)$ using Eq. (13). After that $D^{(t=0)}$ is substituted by $D^{(t=1)}(\varphi, \lambda)$, new $\bar{\rho}^{\text{CRUST}}(\varphi, \lambda)$ and T_{rr}^{CRUST} are computed

and the algorithm is iterated until convergence (the procedure is summarized in Fig. 2).

2.3. Uncertain crustal density

A further improvement to the inversion algorithm can be implemented by considering that one of the most important quantities required to compute the solution, i.e. $\rho^{\text{CRUST}}(\varphi, \lambda, r)$, is not perfectly known. In order to overcome this problem we decide to rescale the density function of each geological province by a constant unknown scale factor h_i . In this way different geological provinces of the same type can have slightly different density functions. The gravitational effect of the crystalline crust, also recalling the correction of Eq. (15), is thus given by:

$$T_{rr}^{\text{CRUST}} = \sum_{i=1}^M [\mathcal{F}(h_i \rho^{\text{CRUST}}(\varphi, \lambda, r) \chi_i(\varphi, \lambda), \bar{D}, D_T^{\text{CRUST}}) + \mathcal{F}(h_i (\bar{\rho}^{\text{CRUST}}(\varphi, \lambda) - \rho^{\text{CRUST}}(\varphi, \lambda, r)) \chi_i(\varphi, \lambda), \bar{D}, D^+)] \quad (18)$$

with $\chi_i = \chi_i(\varphi, \lambda)$ the characteristic function of the i th geological province. In the derivation of the new inversion operator, the dependence of the different functions on the spherical coordinates is omitted for the sake of readability. Being the forward operator \mathcal{F} linear with respect to density, the final reduced signal is given by:

$$T_{rr}^{\bar{D}} = T_{rr}^{\text{RES}} - T_{rr}^{\text{MANTLE}} - \sum_{i=1}^M h_i [\mathcal{F}(\rho^{\text{CRUST}} \chi_i, \bar{D}, D_T^{\text{CRUST}}) - \mathcal{F}(\bar{\rho}^{\text{CRUST}} - \rho^{\text{CRUST}}) \chi_i, \bar{D}, D^+)] \quad (19)$$

and therefore due to the linearity of Eq. (2):

$$\delta \omega = \omega^{\text{RES}} - \omega^{\text{MANTLE}} - \sum_{i=1}^M h_i (\omega_i^{\text{CRUST}} + \delta \omega_i^{\text{CRUST}}) \quad (20)$$

where ω_i^{CRUST} is the (global) contribution of the i th geological province and $\delta \omega_i^{\text{CRUST}}$ is the corresponding correction to account for radial density variations. Substituting Eq. (20) in Eq. (13), we obtain:

$$D(\varphi, \lambda) = \frac{\omega^{\text{RES}} - \omega^{\text{MANTLE}} - \sum_{i=1}^M h_i (\omega_i^{\text{CRUST}} + \delta \omega_i^{\text{CRUST}}) + \mu_\omega}{\rho^{\text{MANTLE}} - \sum_{i=1}^M h_i \bar{\rho}^{\text{CRUST}} \chi_i} + \bar{D}. \quad (21)$$

Note that in Eq. (21) M further unknowns are introduced. Again the solution can be found if we suppose to know the depth of the Moho from external information at least in $M+1$ points (one point for each geological province plus one point for the mean Moho estimation). In particular it is possible to write a set of observation equations with the following form:

$$Y_n^{\text{OBS}} = \sum_{i=1}^M [(D_n^{\text{OBS}} - \bar{D}) \bar{\rho}_n^{\text{CRUST}} \chi_{i,n} - \omega_{i,n}^{\text{CRUST}} - \delta \omega_{i,n}^{\text{CRUST}}] h_i + \mu_\omega \quad (22)$$

where

$$Y_n^{\text{OBS}} = (D_n^{\text{OBS}} - \bar{D}) \rho_n^{\text{MANTLE}} - \omega_n^{\text{RES}} + \omega_n^{\text{MANTLE}} \quad (23)$$

and D_n^{OBS} is the n th Moho depth observation. The subscript n indicates that the function is evaluated at the point of coordinates (φ_n, λ_n) . If the number N of these observations is greater than M , a least

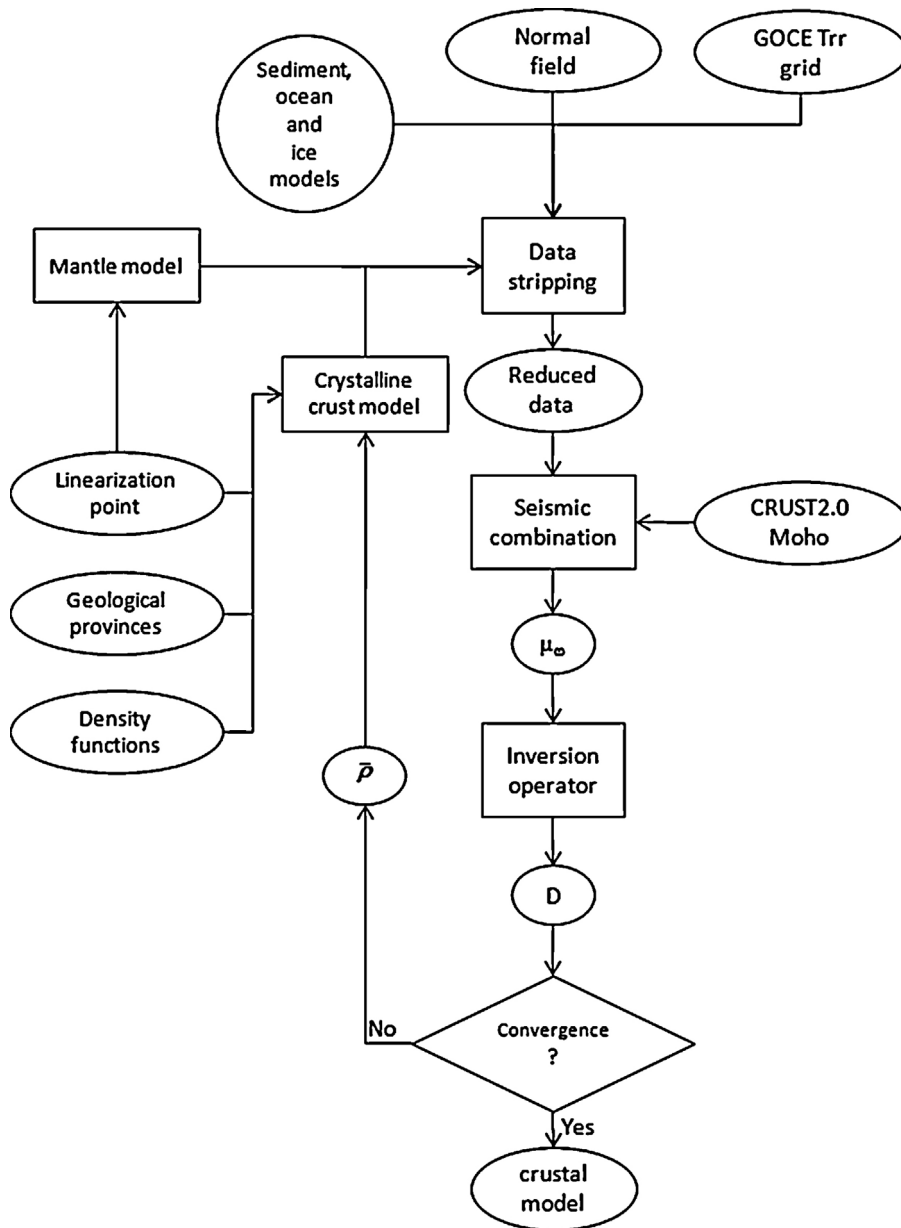


Fig. 2. Schematic representation of the iterative procedure required in order to recover the Moho depth with non-constant crustal density model in the radial direction.

squares adjustment is performed. Actually a Tykhonov regularization is introduced into the least squares minimization principle, i.e.

$$\min_{\mu_\omega, h} \left[\sum_{n=1}^N \frac{(Y_n^{\text{OBS}} - \hat{Y}_n(\mu_\omega, h))^2}{\sigma_n^2} + \alpha_0(\mu_\omega - \tilde{\mu}_\omega)^2 + \sum_{i=1}^M \alpha_i(h_i - 1)^2 \right] \quad (24)$$

where $h = \{h_1, h_2, \dots, h_M\}$, σ_n^2 is the error variance of the n th Moho depth observation, α_i are the regularization parameters (for $i = 0, 1, \dots, M$) and $\tilde{\mu}_\omega$ is a first estimate of the $\delta\omega$ mean value, e.g. using the procedure described in Section 2.1.

Practically the algorithm allows to change the crustal density functions in such a way that the mean depth of each geological province is close to the mean depth obtained by seismic observations. In this respect it is possible to state that the developed algorithm weakly combines gravity and seismic data; we use the

word “weakly” because only few parameters ($M + 1$) are estimated from seismic data for the whole global Moho model.

The least squares estimate of the set of scale factors h should be embedded into the iterative solution presented in Section 2.2, leading to the following inversion operator:

$$D^{(t+1)}(\varphi, \lambda) = \mathcal{I}_3(\delta T_{rr}^{\bar{D}}(\varphi, \lambda), \Delta \rho(\varphi, \lambda), D^{(t)}(\varphi, \lambda), \mu_\omega, h). \quad (25)$$

The system is initialized by considering $D^{(t=0)} = \bar{D}$ and a prior mean crustal density $\bar{\rho}^{\text{CRUST}}(\varphi, \lambda)$. Knowing $D^{(t=0)}$ it is possible to compute T_{rr}^{CRUST} from Eq. (15), reduce and invert the gravitational observations to obtain $\delta\omega$, estimate μ_ω and h using the external information and finally compute $D^{(t=1)}$ using Eq. (21). Once $D^{(t=1)}$ is available, $\bar{\rho}^{\text{CRUST}}(\varphi, \lambda)$ can be updated and the whole procedure is iterated until convergence. In other words, the procedure is the same of that summarized in Fig. 2, but now the output of the seismic combination is not only the estimate of μ_ω but also the ones of h_i , for $i = 1, 2, \dots, M$.

2.4. Reference Moho improvement

All the improvements to the inversion operator introduced up to now do not face the problem that the computed undulation is always referred to a constant Moho depth, even during iterations. This choice, combined to the fact that the inversion operator is linearized around \bar{D} , could lead to a solution whose forward model does not fit very well the original gravity observations.

In order to solve this problem an iterative scheme acting on the Moho depth only and keeping all the other parameters fixed is setup. In particular the values $\hat{\mu}_\omega$ and \hat{h}_i , for $i = 1, 2, \dots, M$, have been previously estimated and therefore the crustal density is now fixed at:

$$\rho_h^{\text{CRUST}}(\varphi, \lambda, r) = \sum_{i=1}^M \hat{h}_i \rho^{\text{CRUST}}(\varphi, \lambda, r) \chi_i(\varphi, \lambda) \quad (26)$$

and

$$\bar{\rho}_h^{\text{CRUST}}(\varphi, \lambda) = \sum_{i=1}^M \hat{h}_i \bar{\rho}^{\text{CRUST}}(\varphi, \lambda) \chi_i(\varphi, \lambda). \quad (27)$$

Making the additional hypothesis that the crustal density below the reference Moho does not depend on the radial direction, recalling that this is already stated for the upper mantle both below and above the reference Moho, i.e.

$$\begin{aligned} \rho^{\text{CRUST}}(\varphi, \lambda, r) &= \bar{\rho}^{\text{CRUST}}(\varphi, \lambda) && \text{for } D > \bar{D} \\ \rho^{\text{MANTLE}}(\varphi, \lambda, r) &= \rho^{\text{MANTLE}}(\varphi, \lambda) && \forall D \end{aligned}, \quad (28)$$

and omitting the dependence of the crustal and upper mantle density functions on the spherical coordinates, Eq. (19) can be rewritten as:

$$\begin{aligned} \delta T_{rr}^{\bar{D}} &= T_{rr}^{\text{RES}} - T_{rr}^{\text{MANTLE}} - \mathcal{F}(\rho_h^{\text{CRUST}}, \bar{D}, D_T^{\text{CRUST}}) - \mathcal{F}(\rho_h^{\text{CRUST}} - \bar{\rho}_h^{\text{CRUST}}, \\ &\quad \bar{D}, D^+) - \mathcal{F}(\rho_h^{\text{CRUST}} - \bar{\rho}_h^{\text{CRUST}}, D^-, \bar{D}) + \mathcal{F}(\rho^{\text{MANTLE}} - \rho^{\text{MANTLE}}, \\ &\quad \bar{D}, D^+) + \mathcal{F}(\rho^{\text{MANTLE}} - \rho^{\text{MANTLE}}, D^-, \bar{D}) \end{aligned} \quad (29)$$

where the surface $D^-(\varphi, \lambda)$ is defined as:

$$D^-(\varphi, \lambda) = \begin{cases} D(\varphi, \lambda) & \text{if } D(\varphi, \lambda) < \bar{D} \\ \bar{D} & \text{if } D(\varphi, \lambda) \geq \bar{D} \end{cases}. \quad (30)$$

Obviously the last three terms in Eq. (29) are equal to zero and therefore it can be rearranged as follows:

$$\begin{aligned} \delta T_{rr}^{\bar{D}} &= T_{rr}^{\text{RES}} - T_{rr}^{\text{MANTLE}} - \mathcal{F}(\rho_h^{\text{CRUST}}, \bar{D}, D_T^{\text{CRUST}}) - \mathcal{F}(\rho^{\text{MANTLE}} - \bar{\rho}_h^{\text{CRUST}}, \\ &\quad \bar{D}, D^+) - \mathcal{F}(\rho_h^{\text{CRUST}} - \rho^{\text{MANTLE}}, D^-, \bar{D}) + \mathcal{F}(\rho^{\text{MANTLE}} - \bar{\rho}_h^{\text{CRUST}}, \\ &\quad \bar{D}, D^+) + \mathcal{F}(\rho_h^{\text{CRUST}} - \rho^{\text{MANTLE}}, D^-, \bar{D}) = T_{rr}^{\text{RES}} - \mathcal{F}(\rho_h^{\text{CRUST}}, \\ &\quad D, D_T^{\text{CRUST}}) - \mathcal{F}(\rho_h^{\text{MANTLE}}, D_B^{\text{MANTLE}}, D) + \mathcal{F}(\rho^{\text{MANTLE}} - \bar{\rho}_h^{\text{CRUST}}, \bar{D}, \\ &\quad D^+) + \mathcal{F}(\rho_h^{\text{CRUST}} - \rho^{\text{MANTLE}}, D^-, \bar{D}) = \delta T_{rr}^D + T_{rr}^{\delta D}, \end{aligned} \quad (31)$$

where

$$\delta T_{rr}^D = T_{rr}^{\text{RES}} - \mathcal{F}(\rho_h^{\text{CRUST}}, D, D_T^{\text{CRUST}}) - \mathcal{F}(\rho_h^{\text{MANTLE}}, D_B^{\text{MANTLE}}, D) \quad (32)$$

is the observation residual with respect to the actual Moho, which is not necessarily at a constant depth, using the radially dependent crustal density, and

$$T_{rr}^{\delta D} = \mathcal{F}(\rho^{\text{MANTLE}} - \bar{\rho}_h^{\text{CRUST}}, \bar{D}, D^+) + \mathcal{F}(\bar{\rho}_h^{\text{CRUST}} - \rho^{\text{MANTLE}}, D^-, \bar{D}) \quad (33)$$

is the signal due to the Moho undulation only, using a mean non-radially dependent crustal density.

By finally applying the iterative inversion operator of Eq. (21) with $\Delta\rho(\varphi, \lambda) = \rho^{\text{MANTLE}} - \bar{\rho}_h^{\text{CRUST}}$, one gets:

$$\begin{aligned} \delta D^{(t+1)}(\varphi, \lambda) &= \mathcal{I}_3 \left(\delta T_{rr}^{\bar{D}}(\varphi, \lambda), \Delta\rho(\varphi, \lambda), D^{(t)}(\varphi, \lambda), \hat{\mu}_\omega, \hat{h} \right) - \bar{D} \\ &= \mathcal{I}_3 \left(\delta T_{rr}^{D^{(t)}}(\varphi, \lambda), \Delta\rho(\varphi, \lambda), D^{(t)}(\varphi, \lambda), \hat{\mu}_\omega, \hat{h} \right) + \delta D^{(t)}(\varphi, \lambda). \end{aligned} \quad (34)$$

This means that the Moho undulation (with respect to a reference Moho at a constant depth \bar{D}) is updated at each step by inverting the residual signal between the observations and the forward model computed from the last iteration Moho.

Note that in the procedures of Sections 2.1, 2.2 and 2.3 the Moho undulation is not updated with smaller and smaller corrections till the forward model is judged satisfactory, but it is iteratively re-estimated from the beginning, just changing some parameters of the inversion operator, such as $\Delta\rho(\varphi, \lambda)$, μ_ω or h .

The procedure of Eq. (34) is initialized by using the Moho undulation and the μ_ω and h parameters obtained at the end of the iterations described in Section 2.3. Once the convergence of Eq. (34) is reached and the final Moho undulation is estimated, one could in principle repeat the procedure of Section 2.3 starting from this final Moho and iteratively improving the estimates of μ_ω and h . This “ping-pong” between parameter estimation (Section 2.3) and Moho refinement (Eq. (34)) can continue till convergence; however, it is not implemented for the GEMMA1.0 model since its impact is negligible.

3. GEMMA Moho estimation

The gravimetric inversion algorithm with all the improvements described in Section 2 is now applied to GOCE data. In particular a grid of second radial derivatives of the gravitational potential at mean altitude of the GOCE satellite is used as input data. This grid was computed by applying the so-called space-wise approach to the satellite tracking and gradiometric observations (Reguzzoni and Tselfes, 2009; Migliaccio et al., 2011): it has a resolution of $0.5^\circ \times 0.5^\circ$ and it is supplied with the corresponding set of Monte Carlo samples of the error grids to be used for covariance modeling (Fig. 3). Note that the grid of second radial derivatives is actually estimated by using all the observed gravity gradients along the orbit within a multi-step collocation scheme.

In the data stripping the following models have been considered. The boundaries of ice sheets, bathymetry and topography (the latter to be used as top of sediments or crystalline crust, depending on the considered region) are taken from ETOPO1 (Amante and Eakins, 2009), while the densities of ice and water are fixed to $\rho^{\text{ICE}} = 980 \text{ kg/m}^3$ and $\rho^{\text{OCE}} = 1020 \text{ kg/m}^3$, respectively. Sediments boundaries and densities are taken from the $1^\circ \times 1^\circ$ model by Laské and Masters (1997). The upper mantle boundaries are defined by two reference surfaces, the former is the reference Moho (i.e. the linearization point) at a constant depth \bar{D} , here assumed equal to 50 km, and the latter is D_B^{MANTLE} , here equal to 123 km (i.e. 100 km below the mean Moho). The upper mantle density $\rho^{\text{MANTLE}}(\varphi, \lambda)$ is taken from Simmons et al. (2010). The effects of lateral density variations in the middle and lower mantle and inside the core are disregarded because they are orders of magnitude smaller than those due to crustal masses and in any case they are mainly concentrated at very long wavelengths (Hager et al., 1985). Finally $\rho^{\text{CRUST}}(\varphi, \lambda, r)$ is modelled in the following way: the Earth crust has been divided into geological provinces according to the USGS map (Exxon, 1995) shown in Fig. 4 (mid-oceanic ridges from Coffin

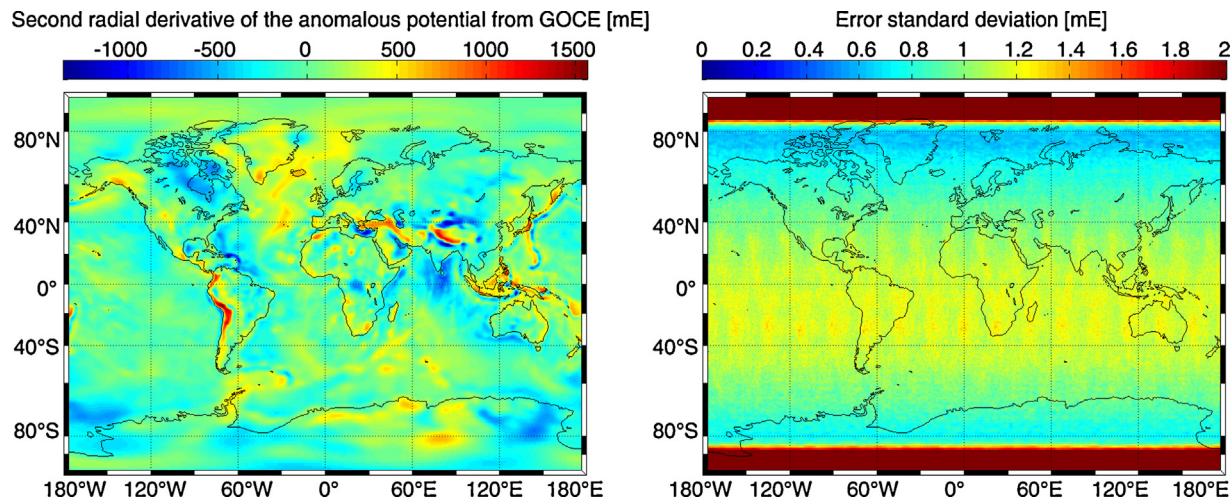


Fig. 3. GOCE grid of second radial derivatives of the anomalous gravitational potential (left) and its error standard deviation (right) from the second release of the space-wise solution (Migliaccio et al., 2011). The error in the GOCE orbit polar gaps is of the order of 20 mE.

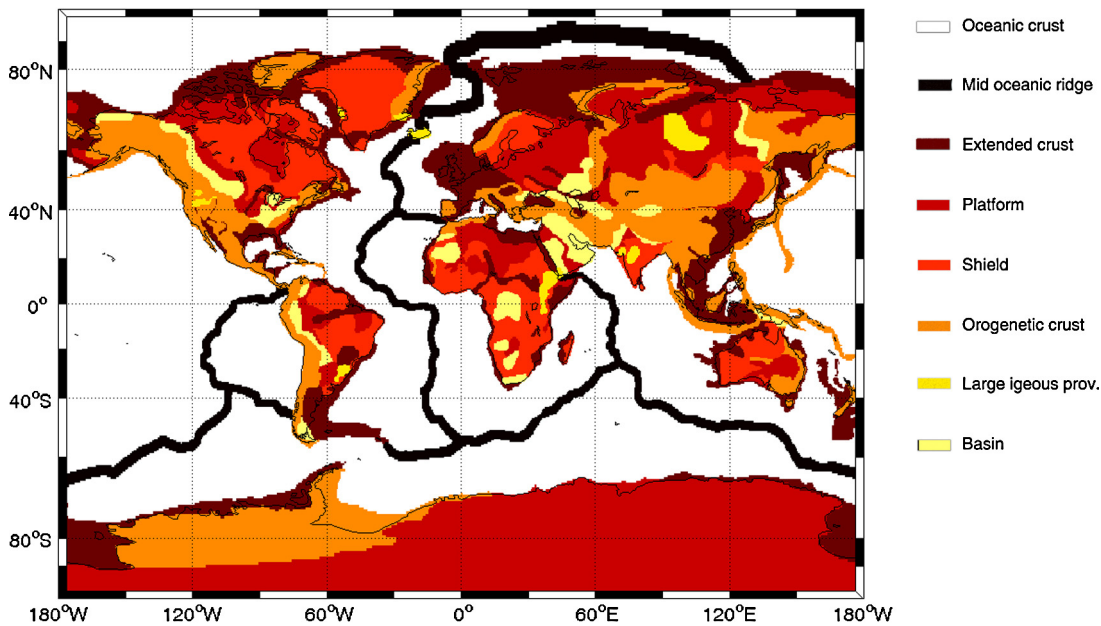


Fig. 4. USGS map of geological provinces enhanced with mid oceanic ridges.

et al. (1998) have been added to the provinces). In this way a set of 139 geologically homogeneous patches has been created, each of them classified as one of the eight main crustal types (i.e. shield, platform, orogeny, basin, large igneous province, extended crust, oceanic crust and mid-oceanic ridge). For each type of province a function relating density to depth is defined (see Fig. 5). These functions are derived from Tables 3 and 8 of Christensen and Mooney (1995) for the continental crust and from Tables 1 and 2 of Carlson and Raskin (1984) for the oceanic crust. The density of mid oceanic ridges is fixed to 2600 kg/m^3 (Lin and Morgan, 1992). Above the sea level the density of the continental crust is fixed to the minimum value of each province. As in Christensen and Mooney (1995) the density of each province is modelled down to a different depth, they have been downward continued by assuming a constant value equal to the maximum available one. Note that this artificial continuation is performed just for the sake of homogenizing the input dataset and it only slightly affects the inversion since in general the continued density is deeper than the Moho discontinuity. In this way below 50 km all the previous densities are constant; this modeling together with the choice of $\bar{D} = 50 \text{ km}$, makes it possible to apply the iterative scheme of Section 2.4.

Once the density and boundaries of each layer are defined it is possible to apply the inversion schemes presented in Section 2. In order to estimate μ_ω and h the CRUST2.0 Moho grid values and their errors, computed as in Reguzzoni et al. (2013), are used as

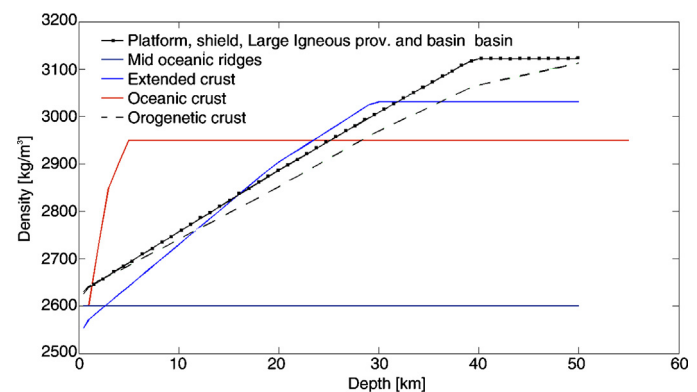


Fig. 5. Densities as a function of depth for the different crustal types.

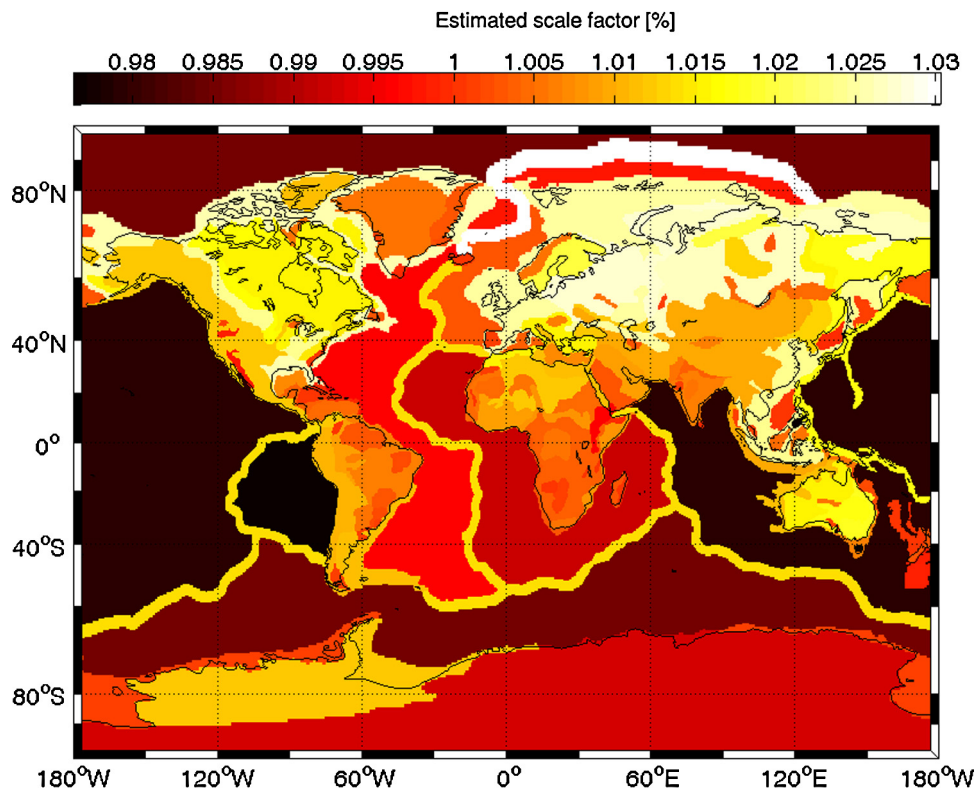


Fig. 6. Least squares estimated scale factors based on CRUST2.0 Moho depths.

additional seismic observations. In this way a set of 16200 new observations (one for each grid-cell of the CRUST2.0 model) is added against 140 unknowns (1 mean value μ_ω plus 139 parameters h_i) thus giving a very high redundancy to the system.

In Table 1 the statistics of the Moho computed by applying \mathcal{I}_0 , \mathcal{I}_1 , \mathcal{I}_2 , \mathcal{I}_3 and the refinement of Section 2.4 (here called \mathcal{I}_4) are presented. It should be reminded that the Moho maps obtained using \mathcal{I}_0 and \mathcal{I}_1 are reported just for the sake of completeness but they

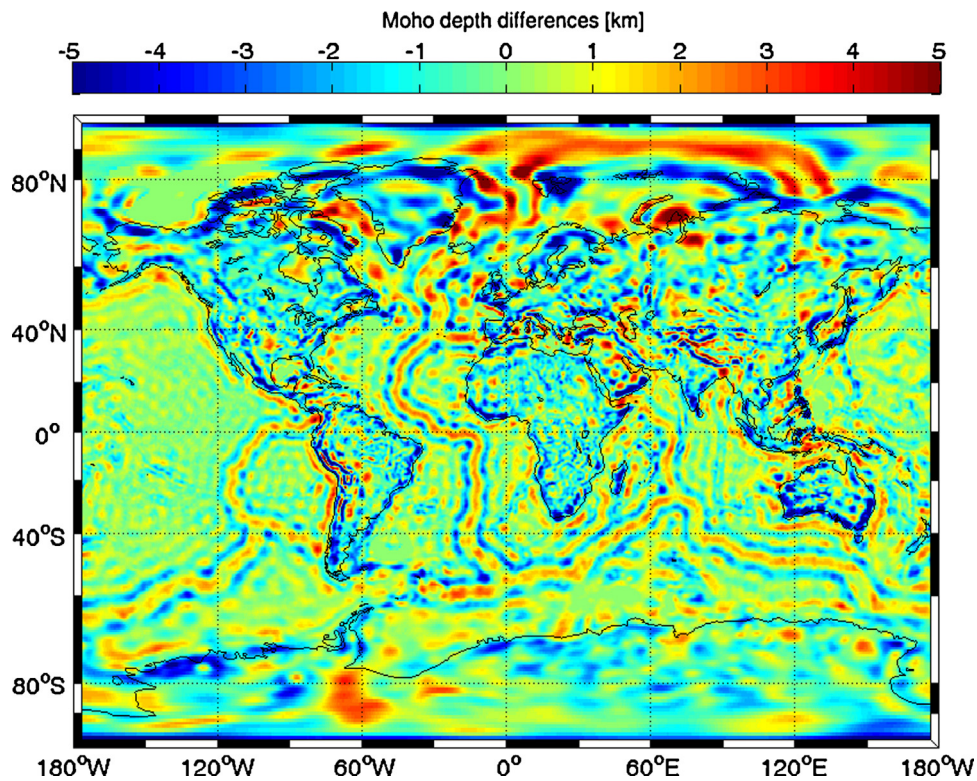


Fig. 7. Differences between \mathcal{I}_3 and \mathcal{I}_4 solutions.

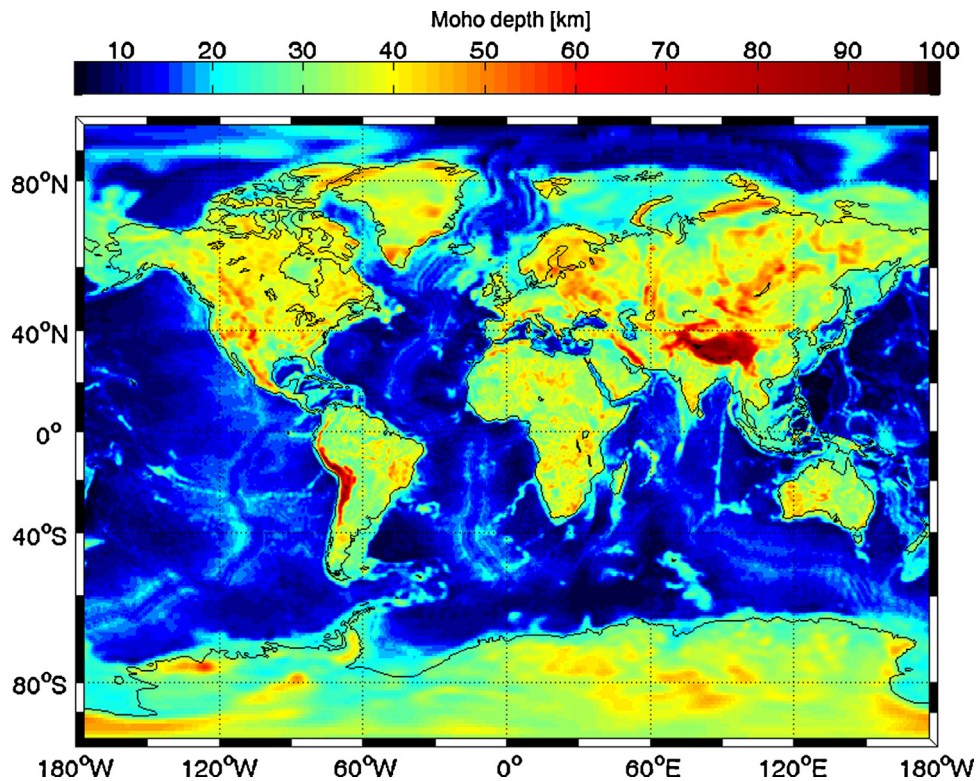


Fig. 8. GEMMA1.0 Moho depth.

contain a logical fallacy due to the fact that the crystalline crustal density used in the data reduction (Eq. (9)) depends on the radial direction too, while the one used for the inversion (Eq. (10)) is supposed to be constant with respect to r .

Looking at the \mathcal{I}_2 solution, i.e. the one that considers the crystalline crust density model as perfectly known, it is interesting to observe that it is quite unrealistic: e.g. it shows a mean depth of about 17 km in the oceanic regions that it is known to be far from the

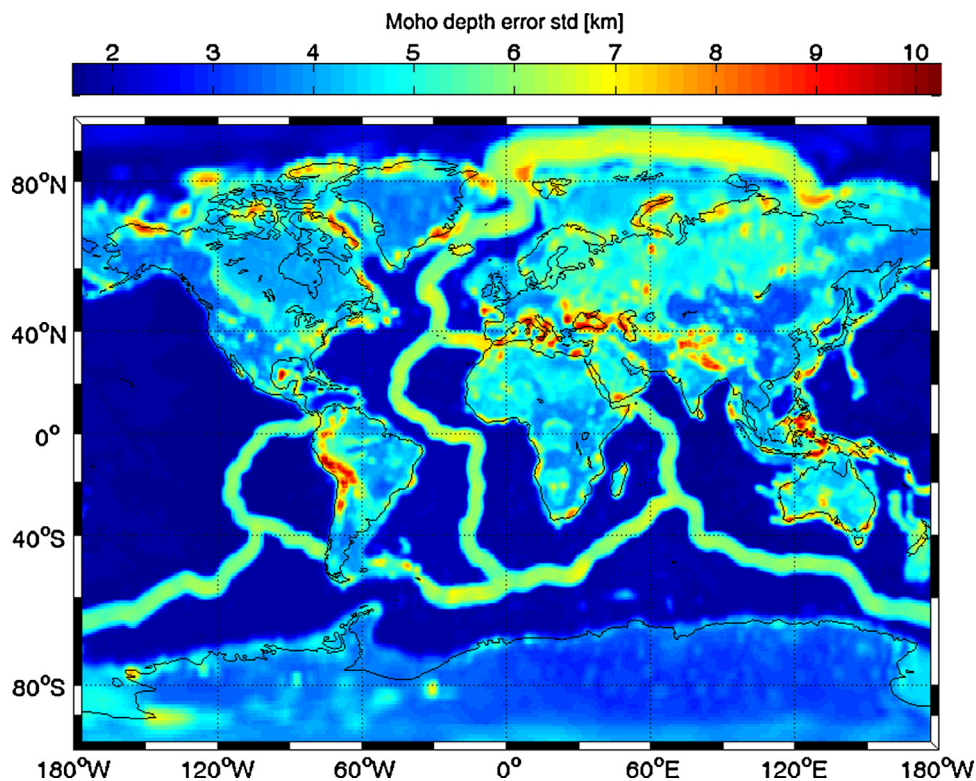


Fig. 9. GEMMA1.0 Moho depth error standard deviation.

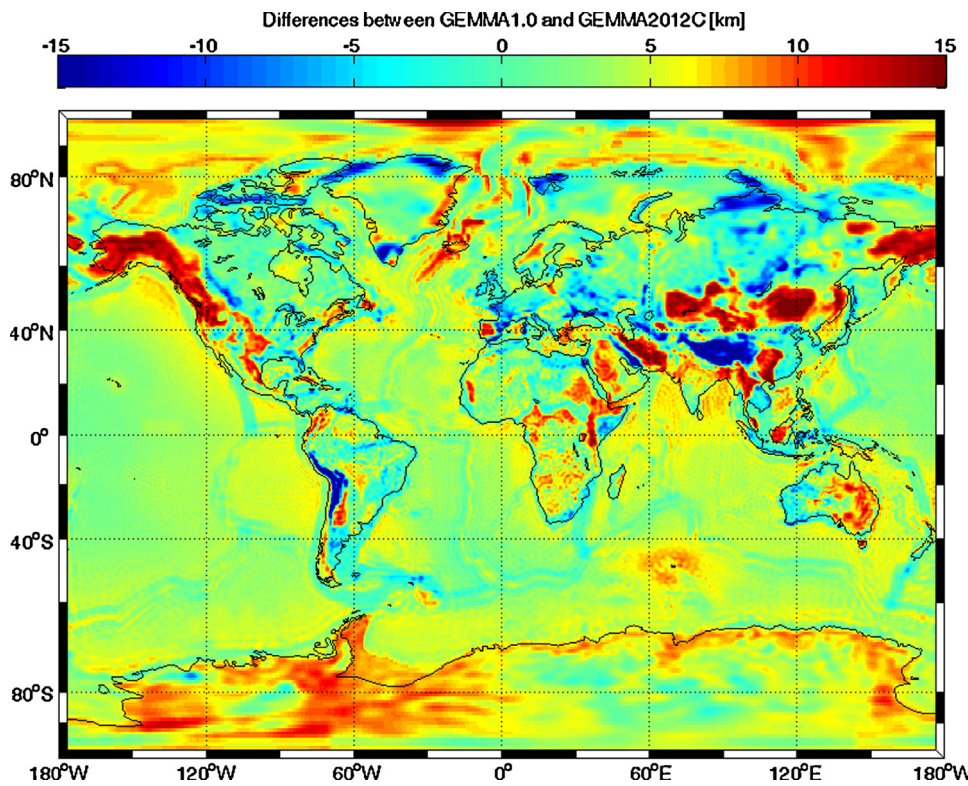


Fig. 10. Differences between GEMMA1.0 and GEMMA2012C.

reality. This means that probably the crustal density structure proposed by Carlson and Raskin (1984) and Christensen and Mooney (1995) are not sufficiently accurate to be used in the inversion of the GOCE gravitational field, thus justifying the introduction of the scale factors h in the \mathcal{I}_3 solution (Fig. 6). It can be seen that in general small corrections are applied: the mean value of the scale factors is 0.996, the maximum one is 1.03 located in the Gakkel Ridge and the minimum one is 0.976 in the young oceanic crust of the Nazca

Plate. Interesting enough is to note that the oceanic crust is in general lightened by the effect of h , while the continental crust is made heavier.

Finally the difference between \mathcal{I}_3 and \mathcal{I}_4 solutions (Fig. 7) clearly shows that the improvement of \mathcal{I}_4 is to recover some high frequencies of the Moho surface (corrections are mainly concentrated in regions with very sharp variation of the Moho depth, like continental margins, orogenetic regions or mid oceanic ridges) that where

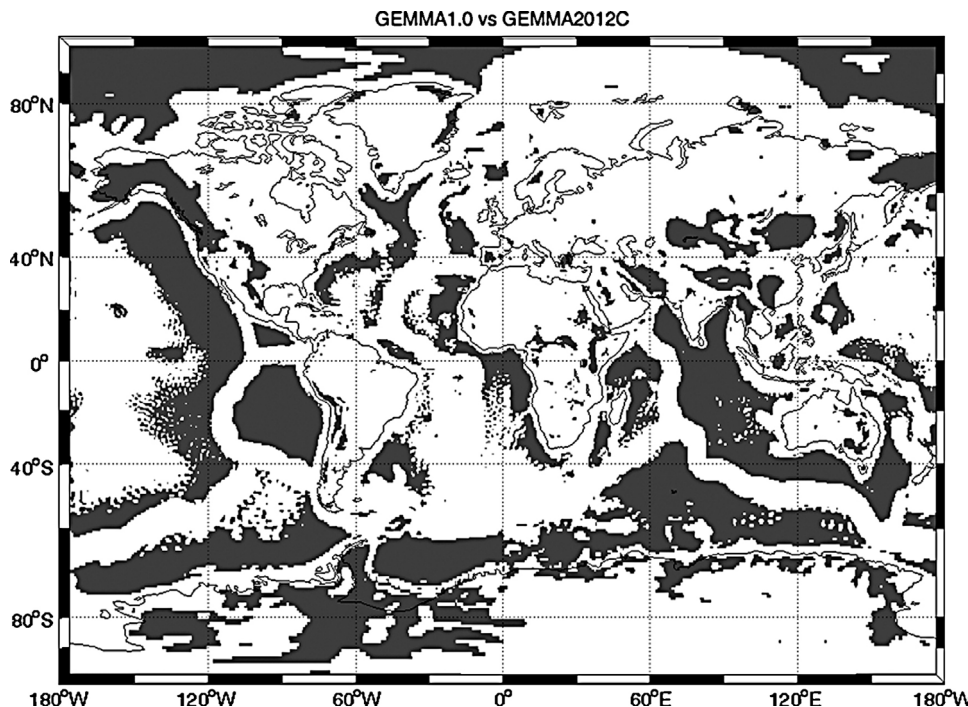


Fig. 11. Coherence map between GEMMA1 and GEMMA2012C global Moho depth models. Grey areas show the regions where the two models are not consistent.

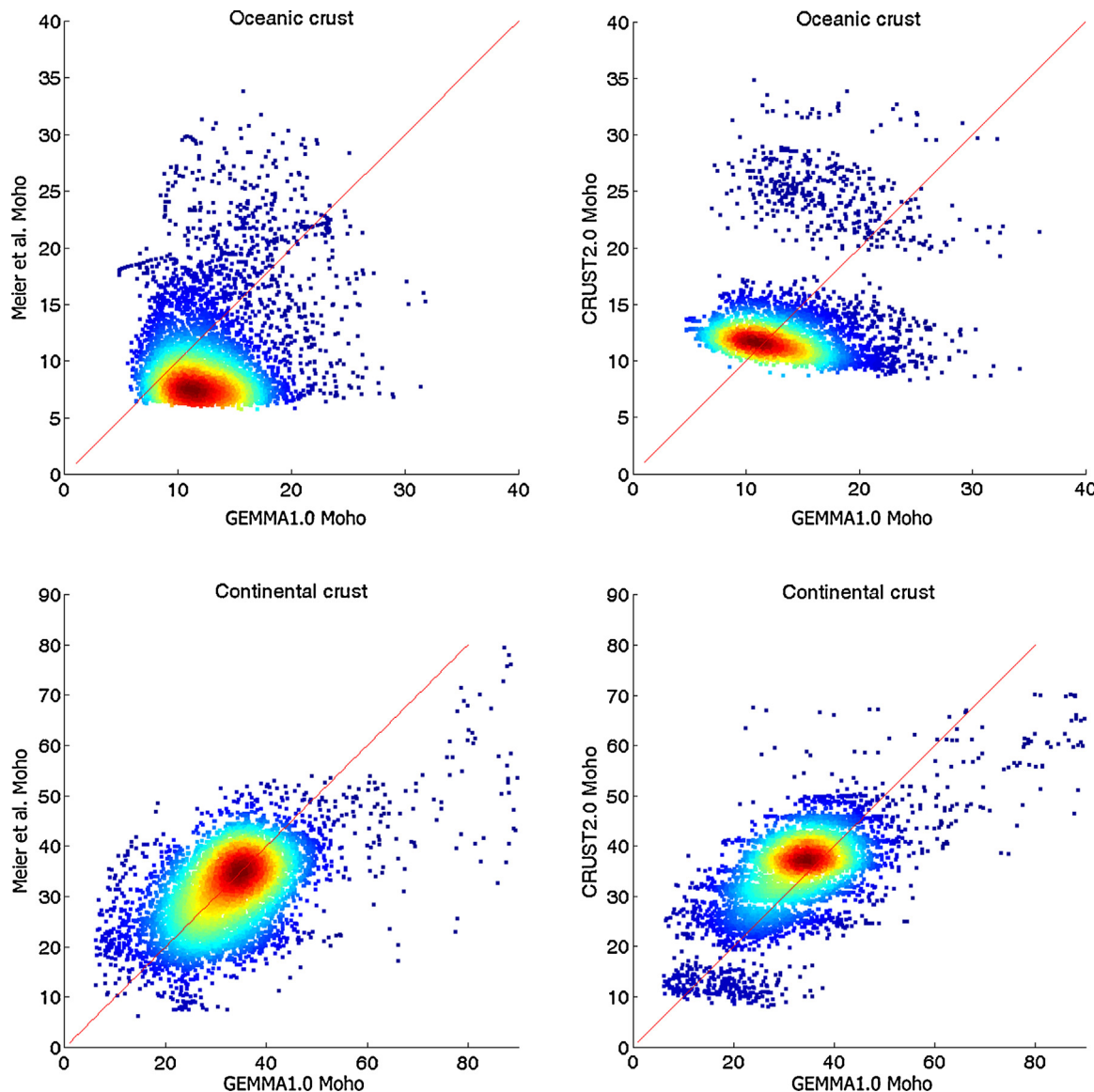


Fig. 12. Comparison between the GEMMA1.0 Moho versus the ones of CRUST2.0 and Meier et al. (2007) for the oceanic and continental crust.

smoothed out by the linearization of the other operators around $\bar{D} = 50$ km. A map of the final GEMMA1.0 global Moho depth is shown in Fig. 8.

The accuracy of the GEMMA1.0 Moho has been empirically evaluated as the sum of different effects. In details the considered error sources are:

1. GOCE observation errors and linearization errors in the inversion operator;
2. errors in the least squares estimation of μ_ω and of h ;
3. model errors in the density functions and in the shape of the geological provinces;

Table 1
Statistics on Moho depths estimated by means of the different inversion operators.

Unit [km]	I_0	I_1	I_2	I_3	I_4
Moho mean	21.6	21.7	22.4	21.3	21.1
Moho std	10.8	10.8	9.9	12.8	12.2
Moho mean (continental crust)	33.7	33.7	33.1	34.5	33.4
Moho mean (oceanic crust)	12.9	12.9	16.9	13.5	12.9

4. errors in upper the mantle density variation.

The first effect has been computed as in Reguzzoni et al. (2013) and shows a global standard deviation of 0.35 km. Errors in μ_ω and h are directly estimated by the least squares solution and have a global standard deviation of 0.8 km. The most important source of error is in the definition of geological provinces. It has been empirically modelled by supposing errors of 0.5° in the definition of the shape of each geological province and an error in the crustal density functions derived again from the uncertainties presented in Christensen and Mooney (1995). The resulting error map has a global standard deviation of 0.9 km. The upper mantle density variation error, computed by supposing an uncertainty of 20% in the mantle density, has a global standard deviation of about 0.35 km. The total error is obtained by summing up all the four different effects, it has a global standard deviation of 1.7 km and it is shown in Fig. 9.

Note that the main unmodelled sources of error are those related to large anomalous regions such as subduction zones or continental convergent plate boundaries where duplications or fragmentations of the Moho can occur. These effects, even if important, are quite

localized and reflect in a wrong Moho depth just very close to the anomaly, as will be further pointed out in Section 4.

At this point it is worthwhile to compare the GEMMA1.0 model with the one computed in Reguzzoni et al. (2013), called GEMMA2012C, in order to numerically evaluate the improvement achieved with the algorithms described in Section 2. A first comparison between the two models shows a mean difference of 4.0 km in the oceanic crust and 3.1 km in the continental one, being GEMMA1.0 closer to the common knowledge about the crustal thickness (Bassin et al., 2000; Huang et al., 2013). Note that this first improvement in the estimate of the mean depth of the continental and oceanic Moho depth cannot be ascribed only to the application of the algorithm presented in Section 2.1, but it is the combined effect of all the upgrades described in Section 2. The differences between the two models have a global standard deviation of 3.9 km and are depicted in Fig. 10. It can be clearly seen the impact of the geological provinces (e.g. in the orogenetic regions) and some residual artefacts of the CRUST2.0 in the GEMMA2012C (e.g. straight edges in Kazakhstan or in the Beaufort Sea). On the other hand, the absence of any modeling of the largest crustal anomalies (e.g. the subduction of the Nazca plate beneath the South American one, or the duplication and fragmentation of the Moho under the Himalayas) leads GEMMA1.0 to a less realistic Moho modeling in those areas than GEMMA2012C, which could take advantage of the direct combination with seismic data without any constraints on the consistency with the gravitational signal. Moreover, looking at the estimated Moho errors, the GEMMA1.0 solution could at first glance appear worse than the GEMMA2012C one, compare Fig. 9 with Fig. 13 in Reguzzoni et al. (2013). However one should also note that neither errors related to the shape and the density variation of the geological provinces, nor errors in the upper mantle density were considered in GEMMA2012C. This led to an underestimate of the Moho depth error standard deviation, that is now more realistic in the GEMMA1.0 model.

These considerations are confirmed by Fig. 11 where statistical inference is used to compare the two models. In particular the comparison is performed taking into account for each grid-cell (i, j) the difference between the Moho depths of the two models, i.e. $\Delta D_{i,j} = D_{i,j}^{\text{GEMMA1.0}} - D_{i,j}^{\text{GEMMA2012C}}$, and supposing that they are independent from one another. In this way the two models are consistent if $\Delta D_{i,j} = 0$ with an error variance $\sigma^2(\Delta D_{i,j}) = \sigma^2(D_{i,j}^{\text{GEMMA1.0}}) + \sigma^2(D_{i,j}^{\text{GEMMA2012C}})$. Assuming a Gaussian distribution of the errors, a simple Z-test can be used in order to verify the hypothesis $\Delta D_{i,j} = 0$ with a confidence level of 95%. The result of this test is shown in Fig. 11 where grey pixels represent the grid cells where the hypothesis is rejected. It turns out that the two models are inconsistent in large part of the oceans (due to the difference in the mean depth of the oceanic crust) and again in correspondence with the largest Earth crustal anomalies, such as subducting plates in North and South America or Himalaya where, as stated before, GEMMA2012C is partially corrected by the direct combination with the CRUST2.0 model.

4. Discussion and conclusions

As it can be seen from Fig. 8 all the major features such as thick continental roots beneath the main mountain ranges as well as the contrast of continental and oceanic crust are retrieved. On a global scale the presented results are in good agreement with the common knowledge about the crustal thickness. To prove this, in Fig. 12 the GEMMA1.0 Moho depth is plotted versus the CRUST2.0 one and a Moho computed by inverting fundamental mode Love and Rayleigh phase and group velocity maps (Meier et al., 2007). In order to compare the models, since both CRUST2.0 and the Moho from Meier

et al. (2007) are delivered on a $2^\circ \times 2^\circ$ grid, the GEMMA1.0 Moho has been first smoothed by means of a moving average and then undersampled to the same resolution of the other models. The first thing that can be observed is that in general CRUST2.0 shows a quantitated scatter plot due to the fact that in large regions, where no seismic data are available, the Moho depth has been fixed to standard values. Apart from that, the GEMMA1.0 oceanic Moho is in good agreement with the CRUST2.0 model, while it is deeper than the one from Meier et al. (2007). On the contrary in the continental crust the GEMMA1.0 model is very well aligned with the model from Meier et al. (2007), while CRUST2.0 shows a deeper Moho. The largest differences with respect to the other two models are concentrated in the Himalayas and in the Andes, this is very likely due to the effect of unmodelled density anomalies. For example the Nazca subduction in South America as well as duplications and fragmentations of the Moho in the Himalayas, both not modeled in GEMMA1.0, are reflected in a thickening of the crust. However it should be noted that in these complicated regions the concept of Moho itself becomes meaningless, since there is not a sharp separation between crust and mantle. A more detailed comparison between the GEMMA1.0 model and other global and regional models is reported in Sampietro et al. (2013). The final model seems to be an improvement of the nowadays widespread CRUST2.0 model for different aspects: first of all the new model, combining GOCE data and CRUST2.0 seismic information (where judged reliable), is well consistent with the actual gravity field, thus overcoming one of the main limitation of seismic derived global models. In particular the gravitational effects of the GEMMA1.0 model differs from GOCE observations by 49 mE while the CRUST2.0 one differs by 1015 mE. Moreover since the used gravity data are acquired by a satellite mission, the Moho is computed from a uniform and homogeneously distributed dataset (differently from CRUST2.0 where large areas are uncovered by seismic observations).

The resulting GEMMA 3D crustal model has a planimetric resolution of $0.5^\circ \times 0.5^\circ$ and a vertical resolution of 1 km, i.e. the used discretization step of the density functions, again improving the state of the art of the global crustal knowledge.

The whole model, i.e. the top and the bottom of each layer, the density distribution and the corresponding gravitational signal is freely available through a web processing service at the web page <http://goceodata.como.polimi.it>.

Acknowledgements

The present research has been partially funded by ESA in the framework of the STSE program through the GOCE Exploitation for Moho Modeling and Applications (GEMMA) project, contract no. 4000102372/10/I-AM.

References

- Amante, C., Eakins, B.W., 2009. ETOPO1 1 arc-minute global relief model: procedures, data sources and analysis, NOAA Technical Memorandum NESDIS NGDC-24, March 2009, 19 pp.
- Bassin, C., Laske, G., Masters, G., 2000. The current limits of resolution for surface wave tomography in North America. *EOS Trans. AGU* 81.
- Braatenberg, C., Mariani, P., Pivetta, T., 2011. GOCE observations in exploration geophysics. In: Proceedings of the 4th International GOCE User Workshop, Technische Universität München (TUM), Munich, Germany (ESA SP-696, July 2011).
- Carlson, R., Raskin, G., 1984. Density of the ocean crust. *Nature* 311, 555–558.
- Christensen, N.I., Mooney, W.D., 1995. Seismic velocity structure and composition of the continental crust: a global view. *J. Geophys. Res.: Solid Earth* 100, 9761–9788.
- Coffin, M., Gahagan, L., Lawver, L., 1998. Present-day plate boundary digital data compilation. Technical Report 174 (5). University of Texas, Institute for Geophysics.
- Colombo, O.L., 1981. Numerical methods for harmonic analysis on the sphere, Report No. 310. Ohio State University, Dept of Geodetic Science.
- Drinkwater, M., Floberghagen, R., Haagmans, R., Muzi, D., Popescu, A., 2003. GOCE: ESA's first Earth Explorer Core mission. *Earth Gravity Field from Space – From*

- Sensors to Earth Sciences, vol. 18. Kluwer Academic Publishers, Dordrecht, Netherlands, pp. 419–432.
- Dziewonski, A.M., Anderson, D.L., 1981. Preliminary reference Earth model. *Phys. Earth Planet. Inter.* 25, 297–356.
- Exxon, 1995. Tectonic Map of the World, 18 sheets, scale 1:10,000,000. Technical Report. Exxon, Houston, TX.
- Fowler, C.M.R., 1990. *The Solid Earth: An Introduction to Global Geophysics*. Cambridge University Press, Cambridge, United Kingdom.
- Gatti, A., Reguzzoni, M., Venuti, G., 2013. The height datum problem and the role of satellite gravity models. *J. Geod.* 87 (1), 15–22.
- Hager, B.H., Clayton, R.W., Richards, M.A., Comer, R.P., Dziewonski, A.M., 1985. Lower mantle heterogeneity, dynamic topography and the geoid. *Nature* 313 (6003), 541–545.
- Strang van Hees, G., 2000. Some elementary relations between mass distributions inside the Earth and the geoid and gravity field. *J. Geodynam.* 29 (1), 111–123.
- Heiskanen, W.A., Moritz, H., 1999. *Physical geodesy* (reprint). Institut of Physical Geodesy, Technical University, Graz, Austria.
- Huang, Y., Chubakov, V., Mantovani, F., Rudnick, R.L., McDonough, W.F., 2013. A reference Earth model for the heat-producing elements and associated geoneutrino flux. *Geochem. Geophys. Geosyst.* 14 (6), 2003–2029.
- Knudsen, P., Bingham, R., Andersen, O., Rio, M.H., 2011. A global mean dynamic topography and ocean circulation estimation using a preliminary GOCE gravity model. *J. Geod.* 85 (11), 861–879.
- Laske, G., Masters, G., 1997. A global digital map of sediment thickness. *Eos Trans. AGU* 78, F483.
- Lin, J., Morgan, J.P., 1992. The spreading rate dependence of three-dimensional mid-ocean ridge gravity structure. *Geophys. Res. Lett.* 19 (1), 13–16.
- Meier, U., Curtis, A., Trampert, J., 2007. Global crustal thickness from neural network inversion of surface wave data. *Geophys. J. Int.* 169 (2), 706–722.
- Migliaccio, F., Reguzzoni, M., Gatti, A., Sansò, F., Herceg, M., 2011. A GOCE-only global gravity field model by the space-wise approach. In: Proceedings of the 4th International GOCE User Workshop, Technische Universität München (TUM), Munich, Germany (ESA SP-696, July 2011).
- Moritz, H., 1990. *The Figure of the Earth. Theoretical Geodesy and the Earth's Interior*. Karlsruhe, Heidelberg/Wichmann, pp. 1990.
- Pail, R., Bruinsma, S., Migliaccio, F., Förste, C., Goiginger, H., Schuh, W.D., Höck, E., Reguzzoni, M., Brockmann, J.M., Abrikosov, O., Veichert, M., Fecher, T., Mayrhofer, R., Krabbe, L., Sansò, F., Tscherning, C.C., 2011. First GOCE gravity field models derived by three different approaches. *J. Geod.* 85 (11), 819–843.
- Reguzzoni, M., 2004. GOCE: the space-wise approach to gravity field determination by satellite gradiometry (Ph.D. Thesis). Politecnico di Milano, Italy.
- Reguzzoni, M., Sampietro, D., 2012. Moho estimation using GOCE data: a numerical simulation. In: Kenyon, S., Pacino, M.C., Marti, U. (Eds.), *Geodesy for Planet Earth. International Association of Geodesy Symposia*, vol. 136. Springer, pp. 205–214.
- Reguzzoni, M., Sampietro, D., Sansò, F., 2013. Global Moho from the combination of the CRUST2.0 model and GOCE data. *Geophys. J. Int.* 195 (1), 222–237.
- Reguzzoni, M., Tselfes, N., 2009. Optimal multi-step collocation: application to the space-wise approach for GOCE data analysis. *J. Geod.* 83 (1), 13–29.
- Rummel, R., 2012. Height unification using GOCE. *J. Geod. Sci.* 2 (4), 355–362.
- Sampietro, D., Reguzzoni, M., Negretti, M., 2013. The GEMMA crustal model: first validation and data distribution. In: *Proceedings of the ESA Living Planet symposium*, Edinburgh, United Kingdom, 2014b (ESA SP-722, December 2013).
- Sampietro, D., Reguzzoni, M., Braatenberg, C., 2014. The GOCE estimated Moho beneath the Tibetan Plateau and Himalaya. In: Rizos, C., Willis, P. (Eds.), *Earth on the Edge: Science for a Sustainable Planet. International Association Geodesy Symposia*, vol. 139. Springer, pp. 391–397.
- Simmons, N.A., Forte, A.M., Boschi, L., Grand, S.P., 2010. GyPSuM: a joint tomographic model of mantle density and seismic wave speeds. *J. Geophys. Res.: Solid Earth* 115 (B12), 1978–2012.
- Sjöberg, L.E., 2009. Solving Vening Meinesz–Moritz inverse problem in isostasy. *Geophys. J. Int.* 179 (3), 1527–1536.
- Sjöberg, L.E., Bagherbandi, M., 2011. A method of estimating the Moho density contrast with a tentative application of EGM08 and CRUST2.0. *Acta Geophys.* 59 (3), 502–525.
- Sünkel, H., 1985. An isostatic Earth model. Report No. 367. Ohio State University, Department of Geodetic Science and Surveying.